Journal of Fluids and Structures 18 (2003) 131–143

JOURNAL OF FLUIDS AND STRUCTURES

www.elsevier.nl/locate/jnlabr/yjfls

Vortex shedding behind a nonparallel pair of circular cylinders

R. Hiramoto[a], H. Higuchi[b,*]

[a] *Department of Mechanical Systems Engineering, Hokkaido Institute of Technology, Sapporo 060-8585, Japan*
[b] *Department of Mechanical, Aerospace and Manufacturing Engingeering, Syracuse University, 151 Link Hall Syracuse, NY 13244-1240, USA*

Received 25 October 2002; accepted 8 July 2003

Abstract

This paper reports on experimental investigations on spanwise variation of vortex shedding behind a pair of circular cylinders placed side-by-side at a small angle between the cylinders. The experiments are conducted in air and in water with Reynolds number 440 based on cylinder diameter. In addition to flow visualization studies, measurements are carried out with the DPIV technique and hot-wire probes. The vortex roll-ups and sheddings are compared with those behind parallel pairs of cylinders. The wake pattern behind the nonparallel pair of cylinders varies in the spanwise direction between the two ends from mostly independent vortex shedding to almost single-body wake structure. At the intermediate spacing, strong wake interactions and biased gap flows are observed. The spatial variation of the time-averaged vortex shedding frequency is similar to those observed behind a parallel pair of circular cylinders corresponding to the local spacing ratios, except for the modified shedding frequency due to flow three-dimensionality. The variation in vortex shedding, however, occurs discretely in the spanwise direction rather than continuously. The boundary between the biased gap flow and the mostly independent vortex shedding is located in the spanwise region where the spacing is slightly above the cylinder diameter. These regions were separated by intermittent and time-dependent vortex bifurcations and locally oblique vortex shedding resulting in spanwise variation of vortex shedding frequency.

1. Introduction

Wake behavior behind a parallel pair of cylinders, placed side-by-side normal to a uniform flow, has been extensively studied in the past (Spivack, 1946; Bearman and Wadcock, 1973; Williamson, 1985; Zdravkovich, 1985; Kim and Durbin, 1988; Peschard and Le Gal, 1996; Sumner et al., 1999). As expected, the wake patterns depend strongly on the spacing between circular cylinders. Zdravkovich (1985) classified the flow patterns into the following regimes: coupled vortex streets, biased gap flow, and single vortex street. At large spacing, $s/d > 1.2$ where s is the gap size and d is the cylinder diameter (i.e., $T/d > 2.2$, where T is the center-to-center distance between the cylinders), two Kármán vortex streets are generated behind each cylinder, whereas at intermediate spacing, $0.2 < s/d < 1.2$, the flow between the cylinders becomes biased, and narrow and wide wakes are formed. In the biased flow, separate vortex shedding frequencies are observed in the narrow and wide wake sides. The biased flow has been observed to be bistable, and the gap flow is subject to flip-flopping at increased Reynolds numbers. At small spacings, $s/d < 0.2$, the wake resembles that seen behind a single body. Unlike circular cylinders, flat plates possess fixed separation points. Nevertheless, similar wake interactions have been observed behind a pair of flat plates placed side-by-side (Hayashi et al., 1986; Miau et al., 1992; Higuchi et al., 1994). The present study adds a new perspective to the problem and addresses the wake interaction problem where the spacing between the cylinders varies continuously along the span.

*Corresponding author.
E-mail address: hhiguchi@syr.edu (H. Higuchi).

0889-9746/$ - see front matter
doi:10.1016/S0889-9746(03)00089-6

The spanwise variation of vortex shedding can also be observed behind a tapered cylinder. The nonparallel outer flow configuration is somewhat analogous to that of a tapered cylinder. Gaster (1969, 1971) was among the first to study vortex shedding from a tapered cylinder. The main interest was how vortex shedding is modulated along span; in the latter paper, cell structures were pointed out as a mechanism of discrete spanwise variation in vortex shedding. Piccirillo and Van Atta (1993) revealed that vortex splits form the boundaries of a cell structure; the cell size can be scaled with the center-span Reynolds number, and the number of cells is a linear function of the degree of taper.

In the present experimental study, the diameter of each cylinder is constant, but the spacing between the two is varied. In other words, the length scale for the primary vortex shedding is fixed, but the degree of interaction varies due to the gradual change in the spacing between the cylinders.

2. Flow configurations and experimental methods

2.1. Wind tunnel and water channel

The experiments were carried out at Tohoku University in a recirculating-type wind tunnel with an open test-section downstream of a 0.29 m wide octagonal jet nozzle. Supplementary qualitative experiments were conducted at Syracuse University in a water channel with a $0.61 \times 0.61\,m^2$ test-section. In both facilities, the Reynolds number, Re, was 440, based on the free-stream velocity and the diameter of a circular cylinder. The free-stream turbulence level of the wind tunnel at 2.2 m/s free-stream velocity used for the present experiment was less than 0.8%. The tunnel typically operates at higher free-stream velocity with lower turbulence level, but the present conditions were deemed adequate for the experiment. The water channel free-stream turbulence was less than 1–2% according to the LDV measurements.

2.2. Arrangement of cylinders and coordinate system

Fig. 1 shows the arrangement of cylinders as viewed from downstream, with the coordinate system superimposed. The experimental conditions and angles and range of spacing between cylinders are given in Table 1. Two angles between the cylinders were tested in air. The configuration with the smaller angle was introduced to focus on the region of high wake interaction. In the water channel experiment, the end of cylinder, $z = 0$, is the test-section wall and the other end protrudes through a free surface. In the wind tunnel experiment, transparent end-walls were used on both ends of cylinders to avoid perturbations from the jet shear layer. As in the earlier water channel experiment with two parallel flat plates (Higuchi et al., 1994), no adverse effect of the free surface was detected. As for the model blockage,

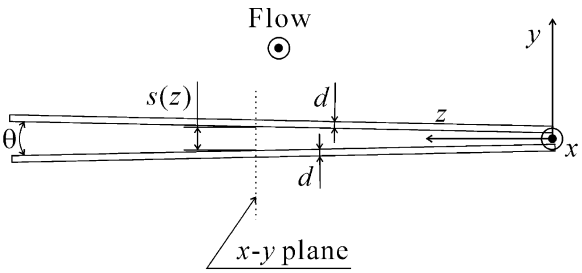

Fig. 1. Cylinder arrangement and coordinate system.

Table 1
Experimental conditions

	Exp. (1) Water channel	Exp. (2) Wind tunnel	Exp. (3) Wind tunnel
U	0.035 m/s (water)	2.2 m/s (air)	2.2 m/s (air)
D	12.7 mm	3 mm	3 mm
Re	440	440	440
Aspect ratio	48	70	70
Spacing ratio s/d	0–1.8	0–3	0.5–1.5
Gap taper angle θ	2.2°	2.4°	0.84°

the sum of the front cross-sectional areas of cylinders corresponded to 2% of the exiting open jet between the end-plates, and 4% of the water channel cross-section.

2.3. Flow visualization and velocity measurement techniques

To visualize the flow, the hydrogen bubble and smoke wire methods were used in water and air, respectively. In the water channel experiment, a SONY Hi8 video camera was used to record sequential vortex shedding illuminated by an overhead projector. In wind tunnel experiments, a SONY DV camcorder and a Nikon D1 digital camera were used to capture the instantaneous flow field illuminated by a light sheet from a 5W Argon-ion laser.

In order to obtain sequential vortex shedding, a high-speed video camera, PHOTRON FASTCAM-Ultima-1, was used. The frame rate in the present experiments was 1125 frames per second with 1/4500 s exposure time.

Hot-wire measurements were performed using one or two single normal hot-wire probes connected to DISA 55M10 anemometers and a band-pass filter (NF Electronic Instruments FV-665). Signals were digitized and processed with an on-line data acquisition system.

Digital particle image velocimetry (DPIV) measurements were carried out with a commercial TSI system consisting of a 1024×1024 pixel CCD camera, a synchronizer, the commercial PIV software together with a New Wave Research Nd:YAG laser. This system on-hand was deemed adequate for the present study, though the amount of the fog seeding was somewhat curtailed to avoid screen contamination.

3. Experimental results

3.1. Cross-sectional views

Individual cross-sectional views resembled those behind parallel cylinders at similar spacings. Three typical types of wake patterns in different $x-y$ planes are shown in Figs. 2–4 as visualized in water. At approximately $s/d > 1.2$, a Kármán vortex street forms behind each cylinder. Because of slight changes in vortex shedding frequency either in time or between two cylinders, in-phase and anti-phase vortex shedding appears, as shown in Figs. 2(a) and (b). The Strouhal number of vortex shedding observed from video motion analysis is approximately 0.2, consistent with the hot-wire measurements presented later.

At another spanwise location with intermediate spacing, shown in Fig. 3, a gap flow between the cylinders deflects toward one side and forms narrow and wide wakes. The flow deflection occurred in either direction in the water channel, but once the flow was established, it was relatively immune to flopping. This observation at the present low Reynolds number is consistent with earlier reports behind a pair of cylinders (Kim and Durbin, 1988). The frequency of outer vortex shedding on the narrow wake side is higher than that on the wide wake side, as will be quantified later. The interaction of vortices occurs downstream of cylinders. Typically the inner vortices, A2 and B1, convect toward the outer vortex, A1, and cause amalgamation among the three vortices. This interaction was reported as the first harmonic mode of vortex shedding from a parallel pair of circular cylinders (Williamson, 1985); in the wake of a parallel pair of circular cylinders arranged in a staggered configuration, a similar interaction is termed "enveloping" (Sumner et al., 2000). In other instances, while the gap-flow deflection remains the same, the vortex B1 is convected downstream past the vortex A2 and its appearance becomes diffused in the region between vortices A1 and B2 as if the gap size were slightly larger. This variation in the flow pattern is believed to be due to the shift in spanwise flow structure, to be addressed in Section 3.5. The global wake pattern downstream remains relatively unaffected by the behavior of the middle vortex.

In the downstream region at a yet smaller spacing ratio $s/d = 0.34$ shown in Fig. 4, the biased gap flow still exists, but the interactions among the vortices corresponding to A1, A2 and B1 in Fig. 3 occur immediately behind the cylinders, and a relatively clear large structure develops further downstream. The wake downstream starts to resemble that usually seen behind a single bluff-body in the intermediate wake region.

3.2. Velocity and vorticity distributions

The results in the remaining sections were obtained in air. Fig. 5 shows mean velocity and turbulence intensity profiles obtained with a hot-wire probe at the downstream station, $x/d = 5.0$, and at several spanwise stations corresponding to $s/d = 0.6$–1.4. The cylinders in this case were set at a narrower angle, $\theta = 0.84°$. The signal was sampled at 10 kHz and averaged over 100 000 points. The jet between cylinders is deflected in a positive y-direction in the figure. In the wind tunnel, the gap flow was observed to be bistable and also subject to artificial disturbance such as brief insertion and removal of a splitter plate in the flow. However, the flow remained stable, from several minutes to

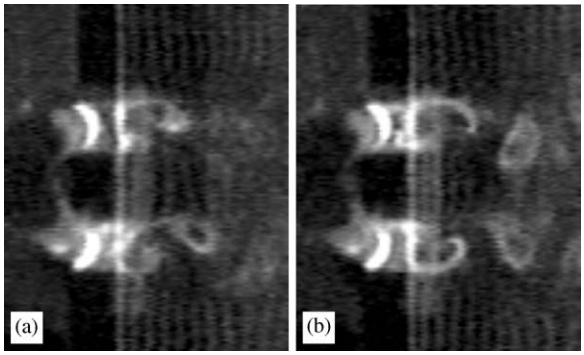

Fig. 2. Hydrogen bubble flow visualizations at $z/d = 39.6$ ($s/d = 1.5$) plane ($\theta = 2.2°$).

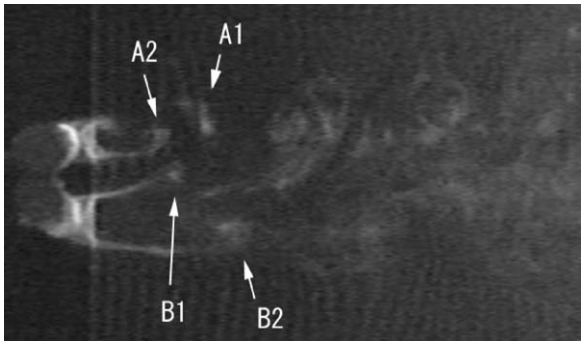

Fig. 3. Hydrogen bubble flow visualizations at $z/d = 18.5$ ($s/d = 0.7$) plane ($\theta = 2.2°$).

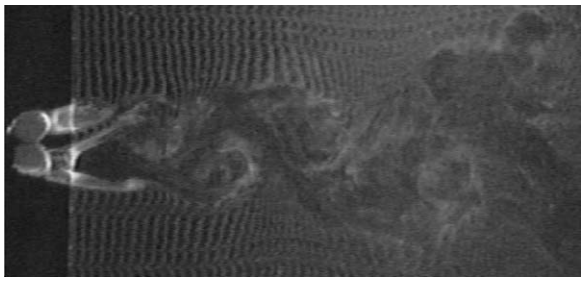

Fig. 4. Hydrogen bubble flow visualizations at $z/d = 7.9$ ($s/d = 0.34$) plane ($\theta = 2.2°$).

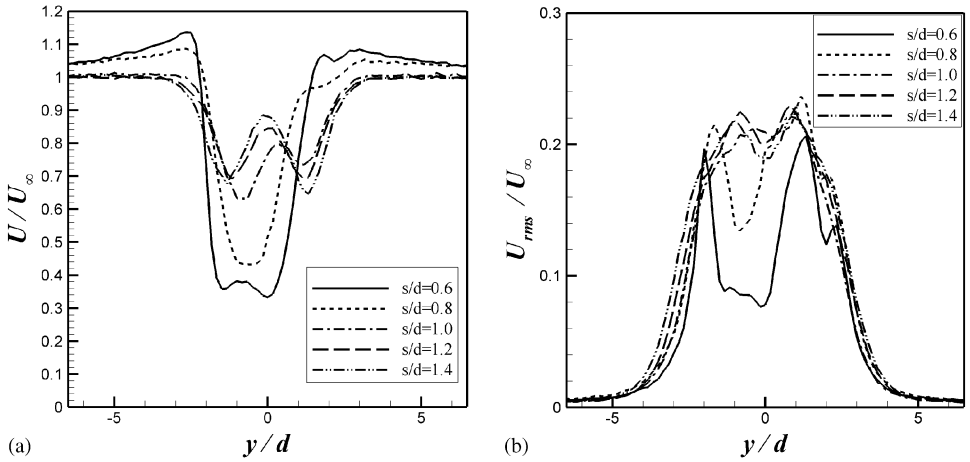

Fig. 5. (a) Mean velocity and (b) turbulence intensity profiles in different spanwise planes at $x/d = 5.0$ ($\theta = 0.84°$).

half an hour, much longer than the duration observed by Kim and Durbin (1988). An additional hot-wire probe in the wake monitored the flow deflection to ensure that the data were collected while the flow was deflected in the same direction. Significant variations among these mean velocity and turbulence profiles are seen, in particular, from $s/d =$ 0.6 to 1.0. The profiles are also dissimilar even within the region between $s/d = 1.0$ and 1.4. It is noted that a single velocity defect pattern corresponds to a double peak in turbulent intensity, and a double peak velocity defect produces a bell-shaped profile.

DPIV measurements in several xy planes were carried out in the air behind the nonparallel pair of circular cylinders ($\theta = 2.4°$) and also behind a parallel pair of circular cylinders ($\theta = 0°$). In Figs. 6 and 7, vorticity distributions are compared for nonparallel and parallel arrangements at spacing ratios $s/d = 1.25$ and 0.75. Individual vortex shedding is more distinct, and less interaction among vortices from two cylinders is seen behind the parallel cylinders. The deflection of gap flow between cylinders persists for a prolonged time behind the nonparallel cylinders at $s/d = 1.25$. However, the gap flow deflection behind the parallel cylinders, as shown in a snapshot in Fig. 6(b), is due to periodic vortex shedding, and there is no mean biased flow. Behind the nonparallel cylinders, the interaction among four vortices identified in Fig. 3 can be seen in Fig. 6(a). By $x/d \approx 5$, the vorticity associated with the vortex B1 is cancelled and/or integrated among vortices A1, A2 and B2. With a smaller spacing of $s/d = 0.75$, the gap flow deflection exists in both cases, as shown in Figs. 7(a) and (b). Behind the nonparallel cylinders, the vorticity associated with the vortex B1 is seen

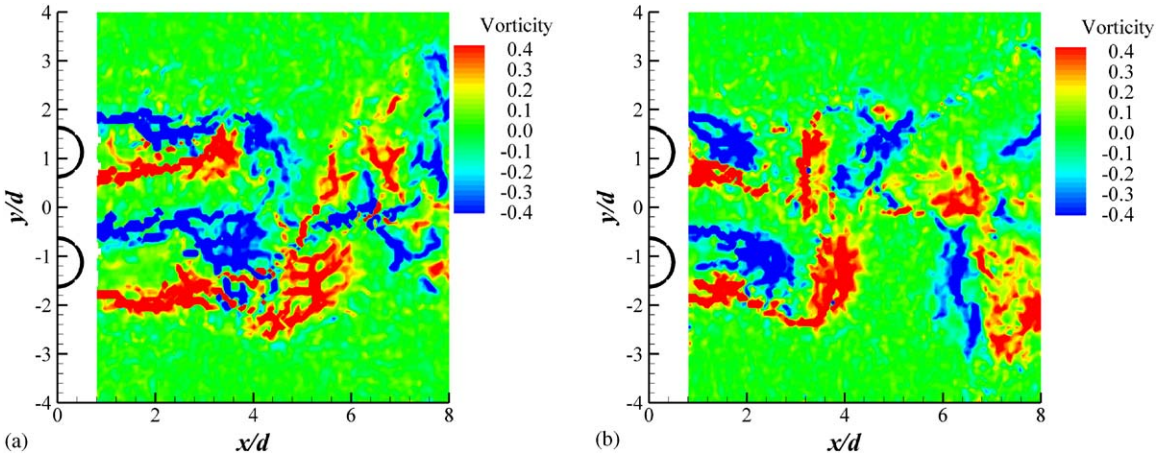

Fig. 6. Comparison of vorticity distributions ($s/d = 1.25$): (a) nonparallel cylinders ($\theta = 2.4°$) at $z/d = 29.3$ and (b) parallel cylinders ($\theta = 0°$).

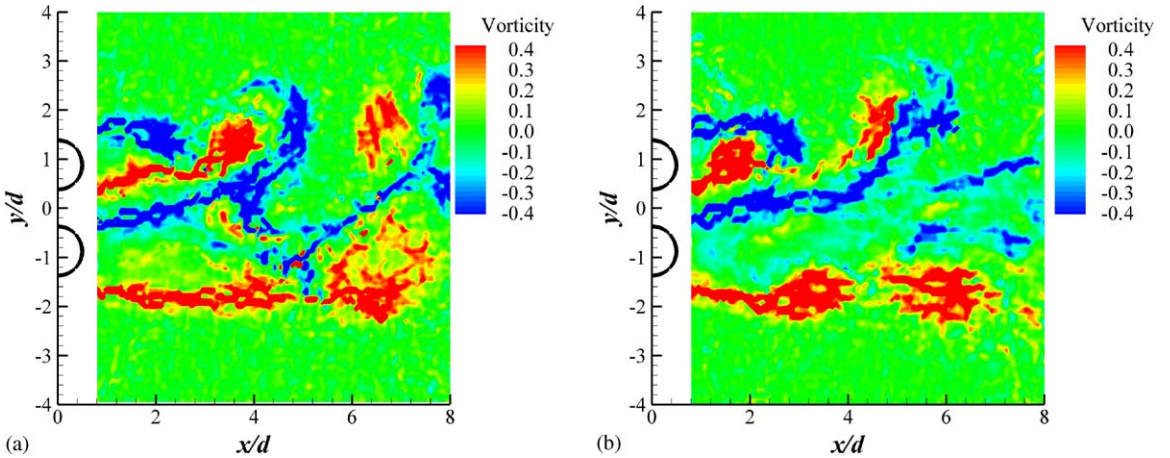

Fig. 7. Comparison of vorticity distributions ($s/d = 0.75$): (a) nonparallel cylinders ($\theta = 2.4°$) at $z/d = 17.6$ and (b) parallel cylinders ($\theta = 0°$).

stretched around A2 in the narrow wake, while it also extends toward B1 in the wider wake. Vortex roll-up and vortex interaction in the wake of nonparallel cylinders occur further downstream than in the case of parallel cylinders, and vorticity in the wake of nonparallel cylinders becomes less concentrated. Fig. 7(b) shows that behind the parallel cylinders the upper, outer shear layer in the intermediate downstream region is formed by the combined A1, A2, and B1 vortices, and the lower shear layer by the vortex B2. Spanwise spacing of vortex shedding will be addressed later together with the shedding frequency.

3.3. Spanwise variation of vortex shedding

The vortex shedding and its spanwise variation were next investigated by visualizing the wake in a plan view and by spanwise scanning of the cross-sectional views. In order to visualize the wake in a plan view, a smoke-wire was located parallel to one of the cylinders with an off-set of 1.0 diameter outside and 1.0 diameter upstream from the cylinder.

Figs. 8(a) and (b) show spanwise formation and shedding of vortices on both narrow and wide wake sides. Threshold-processed images are shown in Figs. 8(c) and (d), and schematics of vortex lines as deduced from the figures are also superposed for reference. In the figures, the flow direction is from left to right, and because the z-axis is normal to the figure, only one cylinder is visible near the left edge of the figure. The cylinders are set at 2.4°, and the spacing ratio, s/d, is 0 at the top of the figure and 3 at the bottom of the figure; ($z/d = 0$ and 70, respectively; refer to Fig. 1) The streamwise spacing between vortices varies along the span. In the wide spacing region, roughly $s/d > 1.5$, and also in the narrower spacing region, roughly $s/d < 0.5$, the sizes of vortices as visualized are similar on both narrow and wide wake sides ((a) and (b)). In contrast, vortex sizes and their streamwise spacings are different between narrow and wide wake sides in the intermediate region, $0.5 < s/d < 1.0$. Relatively small vortices roll up near $x/d = 5.0$ on the narrow wake side at smaller intervals, while intermediate-size vortices can be seen on the wide wake side in the region, $0.5 < s/d < 1.25$ and $x/d > 10.0$. This is consistent with the vortices depicted quantitatively in Fig. 7. In this region the change in structure along the span seems to occur discretely in the form of vortex bifurcations. The bifurcations are visible in this instance near $s/d = 1$ and 1.7 in Figs. 8(a) and near $s/d = 0.6$, 1.2 and 1.5 in Figs. 8(b). Their locations are also marked in Figs. 8(c) and (d). The vortex shedding is not parallel to the cylinder in this region. The structure appears similar to "vortex split" observed behind tapered cylinders by Piccirillo and Van Atta (1993), though cell structures were more numerous in that experiment, since the tapered cylinders affected the primary vortex roll-up. We shall focus our attention in this region. The visualization behind the 0.84°configuration that expands the region near $s/d \approx 1$ will be shown later.

In order to relate the spanwise variation and the cross-flow deflections concurrently, flow visualization was carried out by rapidly scanning a high-speed video camera and a light sheet together in the z-direction. Both the camera and the laser fiber-optic head were mounted on a small traversing carriage underneath the test-section. Four smoke wires were placed upstream and parallel to cylinders to mark the cylinder wakes. In addition, in order to identify the spanwise station of the xy planes, fifteen smoke wires were set in the y-direction, so that when the laser light sheet coincided with individual smoke sheets, the station in the z-direction could be identified. Fig. 9 show scanned xy planes that crossed 15 smoke wires. The scanning speed was slightly slower than the speed required to track the same vortices over multiple

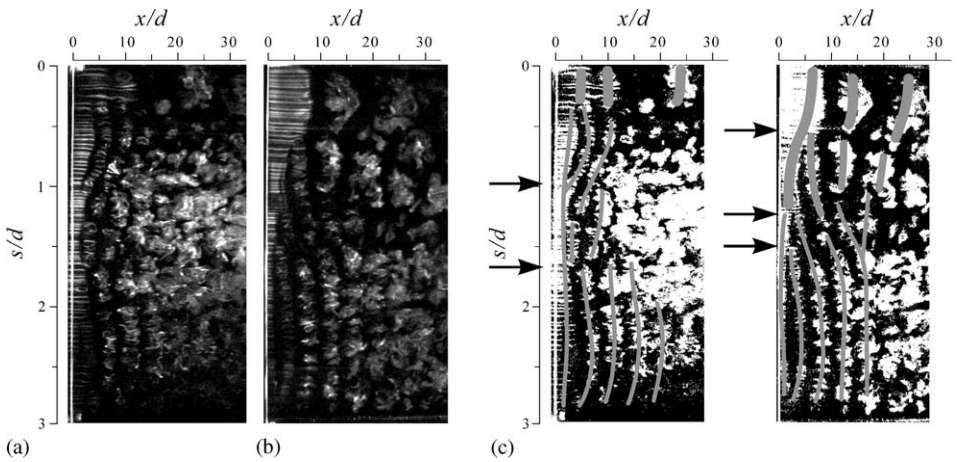

Fig. 8. Top view of the spanwise vortical structure with the $\theta = 2.4°$configuration ($s/d = 0-3$, $z/d = 0-70$): (a) narrow wake side; (b) wide wake side; and (c) schematics of (a) and (b).

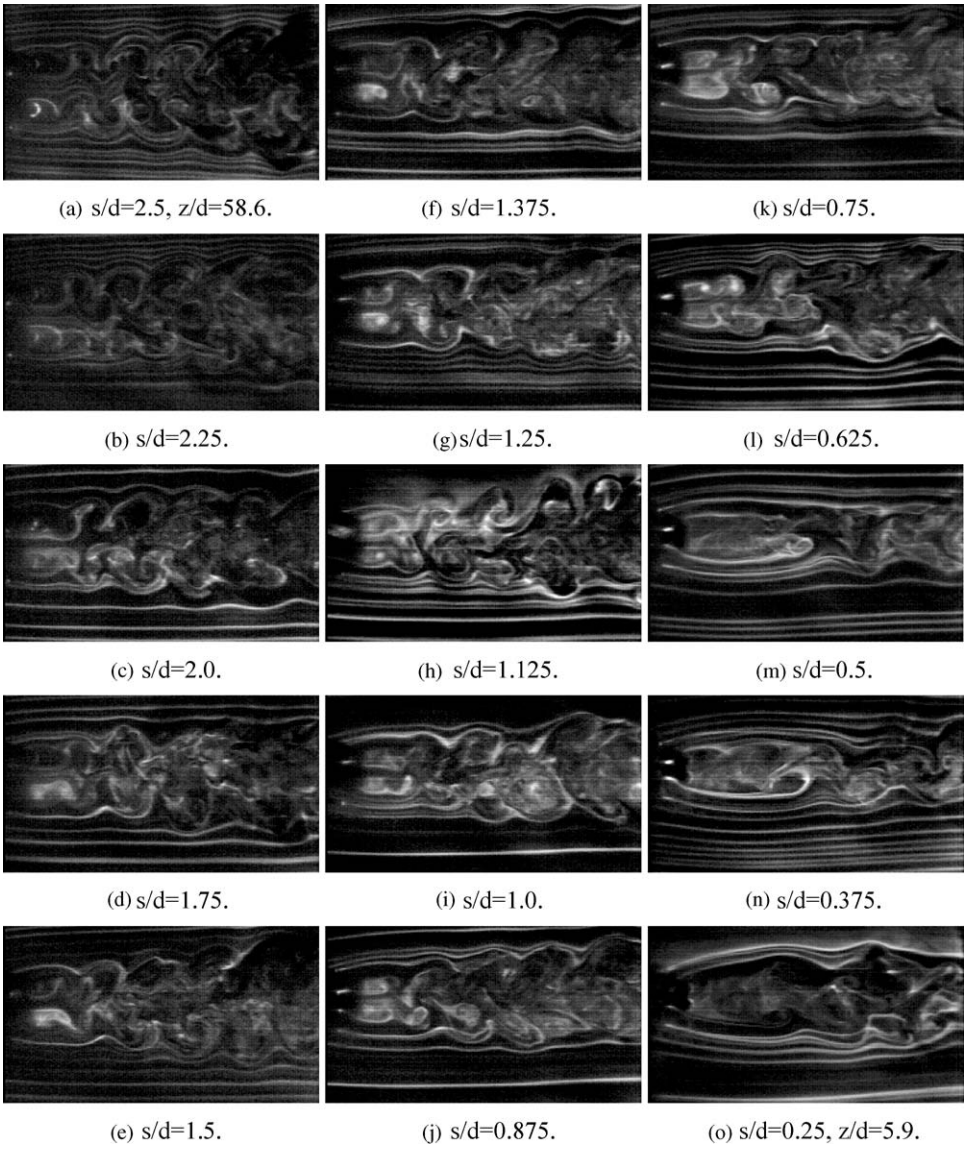

Fig. 9. Spanwise variation of vortex shedding as viewed by rapidly scanning the camera and the light sheet in z-direction ($\theta = 2.4^\circ$).

frames, but was fast enough to avoid flip-flopping of the mean flow. Spanwise transformation of the wake patterns can be seen in considerable detail. For the wide spacing region, $s/d > 1.0$ (Figs. 9(a)–(h)), the size and spacing of vortices on the outer sides are almost identical, and the vortex shedding is nearly in-phase. From $s/d = 0.625$ to 0.5, the wake structure changes rather dramatically. Biased interacting wakes (Fig. 9(l)) evolve toward a single wake with delayed vortex roll-up of the outer shear-layer (Fig. 9(m)). This sudden change of vortical structure is consistent with flow visualization of the spanwise structure shown in Fig. 8 (see, in particular the wide wake side in the similar s/d region). As visualized, for example by outer smoke lines, the vortex shedding frequencies start to differ between two cylinders at $s/d = 0.75$. This region corresponds to $0.5 < s/d < 1.0$ in Fig. 8. Though this trend is not as clearly depicted in Fig. 9(n), examination of other photos taken reveals a biased gap jet at $s/d = 0.375$. Despite differences in visualization technique, a similar flow pattern is observed in water (see Fig. 4). At $s/d = 0.25$, the gap flow is no longer present and the smoke recirculates behind two cylinders. Some three-dimensional flow movement was observed in this region but no definitive conclusion could be drawn. The direction of the deflection of the gap jet was constant across the span within the scan.

Summarizing the results discussed so far, the flow regime in the cross-sectional plane may be categorized into the following regimes with some overlapping regions: single vortex shedding without gap flow for $0<s/d<0.37$; with weak gap flow for $0.37<s/d<0.5$, biased gap flow resulting in narrow and wide wake with asymmetric vortex shedding for $0.5<s/d<1.3$; vortex shedding from each cylinder for $s/d>1.3$. In general, three overall regimes are similar to those behind parallel cylinders as listed by Zdravkovich (1985). However, the discrete three-dimensional structure in the present case prevents one to apply a quasi-two-dimensional approach categorically.

3.4. Power spectra and variation of vortex shedding frequency

In order to quantify the vortex shedding frequency, hot-wire measurements were carried out on both the narrow and wide wake sides. Since the change of vortex shedding was found mainly in $s/d<1.3$ for the 2.4° configuration, the angle between two cylinders was reduced and the spacing variation between cylinders, s/d, was changed in a more moderate range; (see Table 1, $s/d=0.5-1.5$, $\theta=0.84°$.) It was hoped that the complex flow structure in this range could be revealed with enough spanwise length. Again, the second monitoring probe was placed near mid-span to ensure that there was no global switching of the flow pattern during the measurements. Each signal was sampled at 10 kHz for 10 s.

Fig. 10 show the power spectra with $\theta=0.84°$. Spanwise variations of the spectral peaks can be seen on both sides of the wake. In Fig. 10(a), on the narrow wake side, there are clear peaks both at smaller and larger spacing regions. The spectral peak frequency at the smaller spacing decreases almost continuously with increasing spacing, until the relatively broad spectra develop at $s/d\approx0.9-1.3$. On the other hand, throughout all spacings on the wide wake side, the power spectra are broader, with lower peaks, than in the narrow wake side. In particular, double peak spectra can be noted near $s/d=1.0$ on the wide wake side, and a survey with much finer spanwise increments revealed that the spectral peak frequency tended to jump across this spacing region. Both the spanwise movement of the wake and the irregular vortex interactions in the cross-sectional plane are responsible for the spectral variations. Higuchi et al. (1994), demonstrated the nature of the nonperiodic and multiscale vortex shedding behind a pair of flat plates, particularly on the wide wake side, from the results of wavelet analysis and those of conditional spectral analysis. Velocity time-history will be shown below in two selected stations.

The results obtained from the spectral peak measurements are plotted in Fig. 11 and compared with those for $\theta=2.4°$ cylinder configuration. They both show a similar trend: as the spacing is reduced along the span, the Strouhal number resulting from independent vortex shedding, $St\approx0.2$, starts to bifurcate for narrow and wide wake sides. When the spacing is reduced to near zero, only the lower branch of the Strouhal number corresponding to a single-body vortex shedding is observed. The difference between two θ angles is primarily in the position of the bifurcation near $s/d\approx1.2$. Jitter in the waveforms is noted in this region, resulting in a broader peak or double peaks in the power spectra in Fig. 10. This is likely caused by movement of the boundary between the regions with regular and irregular vortex shedding. When the spectra were surveyed with fine spanwise increments, the wide wake side exhibited discrete jump in frequency, while the narrow wake side showed more continuous frequency variation, with a broadening of the spectra near $s/d=1$.

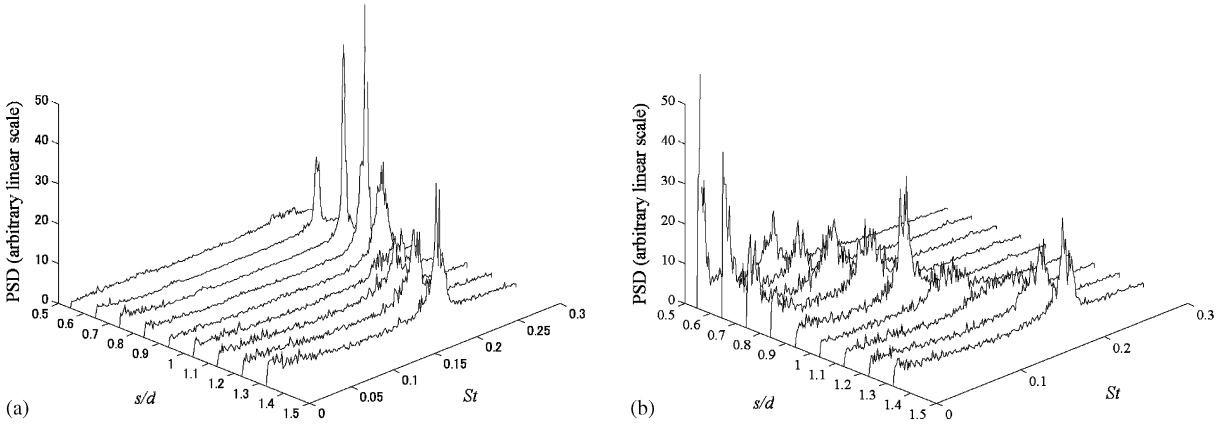

Fig. 10. Spanwise variation of power spectra ($\theta=0.84°$); (hot-wire probe moved in z-direction along $x/d=5$ and $y/d=2$). (a) narrow wake side and (b) wide wake side.

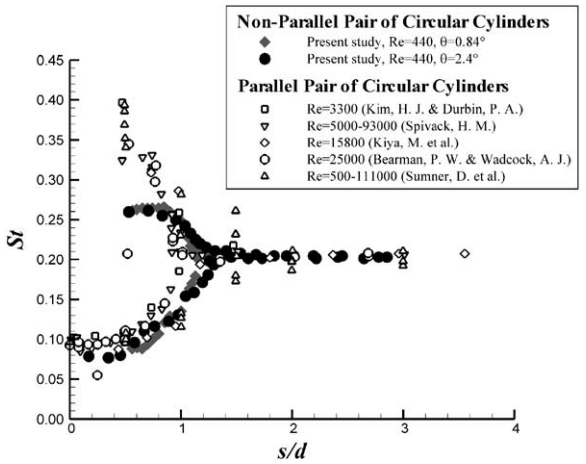

Fig. 11. Spanwise variation of vortex shedding frequency (nonparallel pair of circular cylinders, $\theta = 2.4^\circ$ and 0.84°).

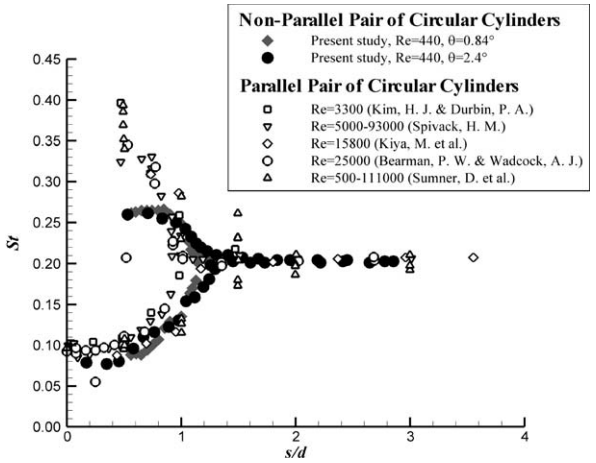

Fig. 12. Vortex shedding frequency versus spacing ratio (comparison between nonparallel and parallel cylinders).

In Fig. 12, the vortex shedding frequency behind the nonparallel pair of cylinders is compared with published data for the two-dimensional case, behind a parallel pair of circular cylinders at different spacing ratios. Note that the present data are taken at different spanwise stations of the fixed configuration, representing the spatial structure of the vortex shedding, while the parallel cylinder data are from different realizations.

The value of s/d at the bifurcation point, where the Strouhal number splits corresponding to the narrow and wake sides, is lower behind the parallel cylinders. The value increases for the $\theta = 0.84^\circ$ case and the $\theta = 2.4^\circ$ case in that order, giving the latter a wider wake interaction region with a greater three-dimensional effect. The frequency of the present result on the narrow wake side, i.e., the higher frequency side, is much smaller than that behind parallel cylinders. The same trend can be seen on the wide wake side. The vorticity field measured with the PIV in Fig. 6 indicated more independent vortex shedding behind parallel cylinders at $s/d = 1.25$. The spacing between the shed vortices on the narrow wake side as shown in Figs. 7 is smaller behind the parallel cylinders. Though the vorticity fields in Figs. 6 and 7 are instantaneous snapshots, the observations are consistent with the time-averaged frequency variations shown in Fig. 12. It is stipulated that the three-dimensional cylinder arrangement and the spanwise flow reduce the strength of the gap jet in the cross-flow plane. Less strength in the vortex roll-up has been noted in the vorticity field, as shown in Fig. 7. In comparison, stronger vortex roll-up and the narrower wake behind the parallel cylinders resulted in the higher Strouhal number. Behind the parallel cylinders, the Strouhal number at $s/d \approx 0$ is half of that at large s/d and corresponds better to a single constant-diameter body than in the nonparallel configuration. In the

region of near-zero spacing between nonparallel cylinders that resemble a tapered body, the flow is subject to both intrinsic flow three-dimensionality and three-dimensionality associated with end conditions. In the wake of a single tapered cylinder, for example, Piccirillo and Van Atta (1993) used the mid-point diameter of the cell structure to normalize the shedding frequency. Behind a cylinder of a constant diameter, end-effects also reduced vortex shedding frequencies (Gerich and Eckelmann, 1982), but in the present case the end-effects on shedding frequency were observed in far more limited regions than in the constant-diameter studies. In spite of geometrical differences, the data in Fig. 12 indicate a similar trend of vortex shedding frequencies between parallel cylinders and nonparallel cylinders. A larger scatter of frequencies in the two-dimensional configuration may be due to diverse sets of data in literature, each containing separate experimental realizations. Differences in the interaction modes reported in these studies may also result in variability in the frequency data.

3.5. Spanwise discrete structures

Spanwise vortical flow visualization has been shown in Fig. 8 for the larger angle between the cylinders. Spectral measurements shown in Figs. 10 and 11 suggested the boundary of spanwise regions near $s/d = 1$. At the lower angle, this intermediate region can be viewed in an expanded manner for $s/d = 0.5-1.5$ instead of $s/d = 0.0-3.0$ for the same cylinder aspect ratio. The flow visualization of the spanwise structure of the moderate arrangement ($\theta = 0.84^\circ$) is shown in Fig. 13. (This particular set of photos was taken at a slightly lower Reynolds number, as indicated.) Step changes in the spanwise structure forming cell structures are seen, and the shedding is not parallel to the cylinders, in particular at $s/d = 0.5-1.0$ on the narrow wake side (Fig. 13(a)). Records of video and other instantaneous images indicate that the cell boundaries near $s/d = 1$ as well as the angle of oblique shedding continue to vary with time.

Fig. 14 shows simultaneous velocity time-histories measured by two hot-wire probes at $x/d = 5$ and $y/d = 2$ separated in the spanwise direction. Two probes are believed to be straddling two cell structures that vary with time. Velocity fluctuations exhibit nonperiodic characteristics and a difference in vortex shedding frequencies is clear even for this small spanwise separation.

In order to ascertain spanwise structure further, space–time correlations of velocity fluctuations at two separate points along the span were obtained. A reference probe was fixed at specified positions and another hot-wire probe was traversed along the span away from the reference probe. The signal length was 20 s sampled at 10 kHz. Cross-correlation functions with respect to the time delay, τ, are mapped out in Fig. 15 against separation, Δz, between the hot-wire probes. The spanwise position of the reference probe in terms of the spacing ratio is indicated in each figure caption. The vortex shedding frequency is clear from the time interval between peaks. In Fig. 15, the variation of intervals on the narrow wake side agrees with the frequency variation revealed in Figs. 11 and 12. The highest spanwise correlation exists in the region of small spacing between the cylinders ($s/d \approx 0.6$). The correlation on the narrow wake side is stronger than that on the wide wake side in the same region. The spanwise correlation becomes weak at $s/d \approx 1.0$ on both sides, and so does the timewise correlation, particularly on the wide wake side, which is consistent with the earlier observations. The location of the weakest correlation corresponds to the station where the frequencies on both sides converge and reach $\mathrm{St} = 0.2$ as shown in Fig. 12, where this point was subject to substantial jittering. Therefore, the results suggest short spanwise structures with fluctuating vortex shedding frequency.

In all the correlation maps except at $s/d = 1.2$, curved or oblique space–time patterns can be seen. Taking a simplified view of the vortex structure, we may relate these patterns to oblique and curved vortex shedding. It is noted that the inclinations of the patterns at $s/d = 0.8$ and 1.0 are opposite on the narrow and wide wake sides. To verify the inclination of vortex shedding, another set of hot-wire measurements was carried out. The reference probe was fixed at a given spanwise position and the second probe, separated by a small spanwise distance, $\Delta z/d = 4$, from the reference probe, was traversed in the streamwise, x, direction to mark the maximum correlation position. The inclination angle of vortex shedding was estimated from the positions of maximum correlation, and the results are given in Table 2. Referring to Fig. 13, positive angle is measured clockwise from the z-axis. (Relatively large estimated uncertainty is due to the probe size, proximity between the probes, and the accuracy of the positioning device.) The results show that the vortex shedding is inclined in opposite directions at $s/d = 0.8-1.0$ which is consistent with Fig. 15, though the angle is not as clear in the flow visualization. There is an indication that vortex interactions occur in different combinations of vortices at various spanwise stations. These are evidenced by bifurcations of spanwise vortices, as seen in Fig. 13, causing step-like spanwise changes in vortex shedding patterns.

In summary, the flow regimes observed in the cross-sectional planes are linked in the spanwise direction, from individual vortex shedding at the large spacings, to the highly biased-wake, and to a single-body vortex shedding, as evidenced in Figs. 9 and 11. The planview flow visualizations and the space–time correlations of the velocity fluctuations revealed that the spanwise variations occur in sections with discrete structural change near $s/d = 1.0$. Curved or oblique vortices are observed between discrete spanwise regions.

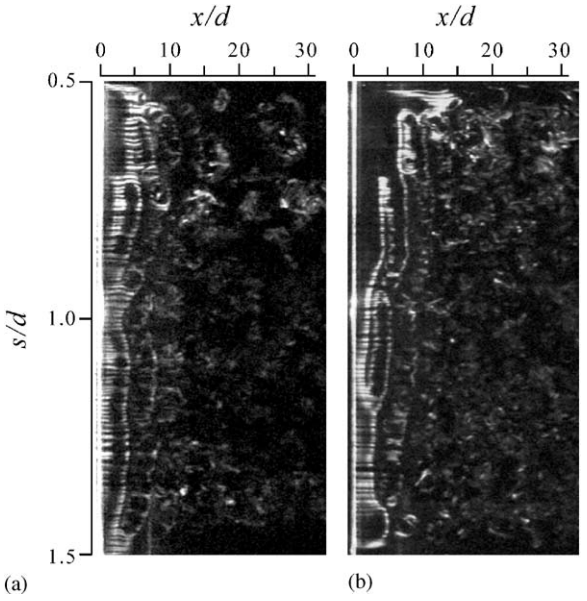

Fig. 13. Spanwise vortical structure with the $\theta = 0.84°$configuration (Re = 360, $s/d = 0.5-1.5$, $z/d = 0-70$). (a) Narrow wake side and (b) wide wake side.

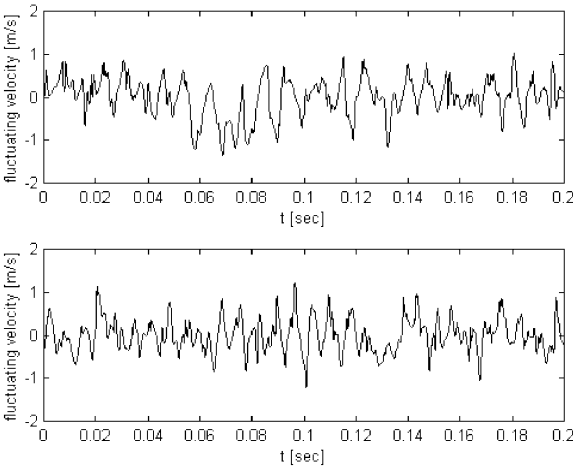

Fig. 14. Waveforms measured simultaneously with $\theta = 0.84°$, at $z/d = 26$ and 34 ($s/d = 0.88$ and 1.0).

4. Conclusions

Three-dimensional vortex shedding and interactions behind a nonparallel pair of cylinders were investigated experimentally. Two angles between the cylinders were examined and the results were compared with the case of parallel cylinders. The flow pattern varied from nearly independent vortex shedding from each cylinder to a biased wake pattern as the spacing decreased in the spanwise direction. The time-averaged vortex shedding frequency varied with the spacing ratio in this region. While the general trend was similar to that behind parallel cylinders, the differences in shedding frequency and in the spacing for the independent vortex shedding are attributed to the three-dimensional nature of the gap flow, in particular at $s/d < 1.0$. The vortex interactions go through step-like changes in this spanwise region, resulting in irregular, time-dependent vortex shedding. Separate spanwise regions were linked by the localized oblique vortex shedding which leads to bifurcations of the vortex structure.

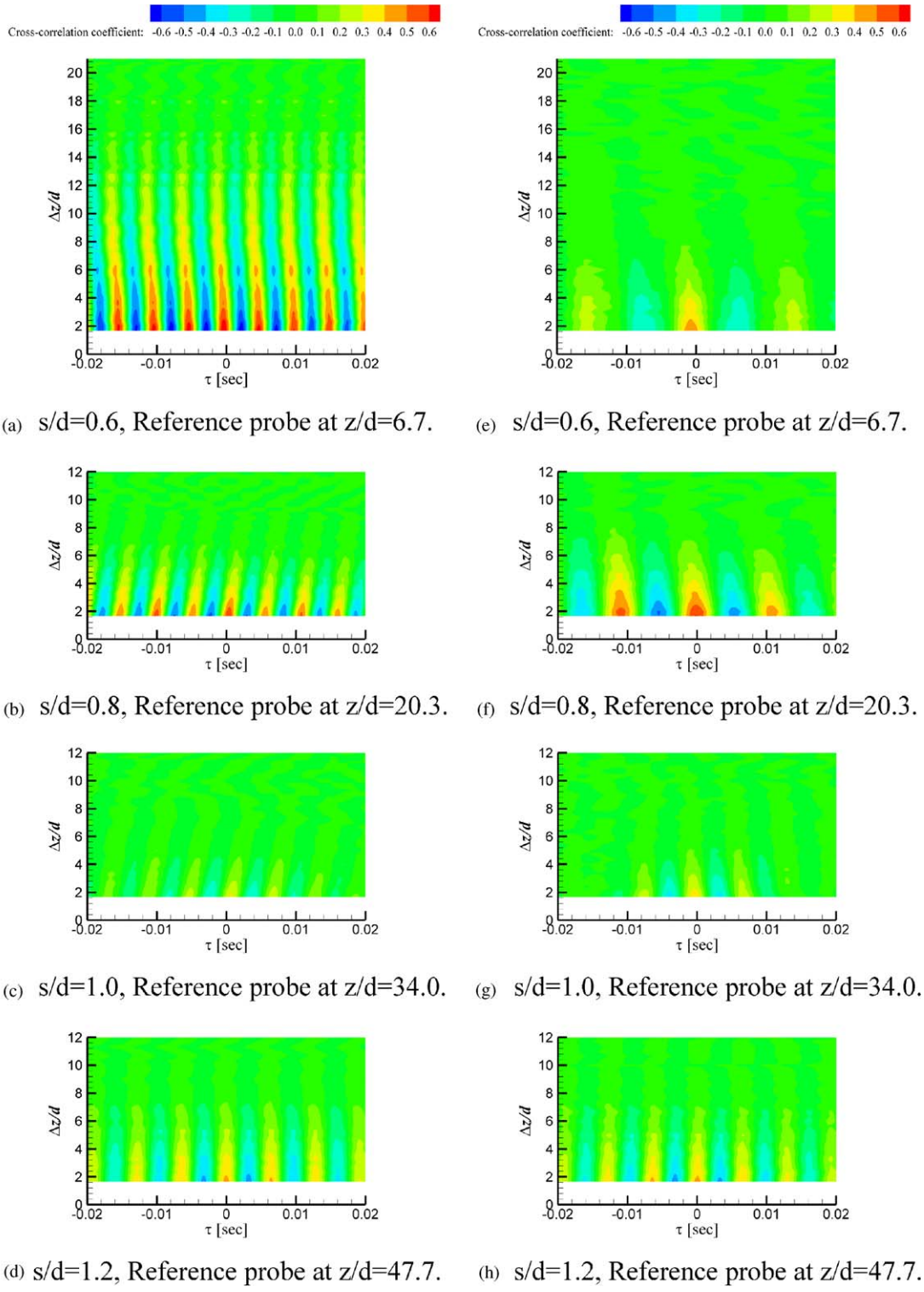

Fig. 15. Space–time correlation with different reference probe positions ($\theta = 0.84^\circ$ $x/d = 5$ and $y/d = 2.5$): (a)–(d) narrow wake side and (e)–(h) wide wake side.

Table 2
Angle of vortex shedding ($\theta = 0.84°$)

s/d	Narrow wake side angle (deg)	Wide wake side angle (deg)
0.6	−3	−2
0.7	−3	−3
0.8	10	−5
0.9	12	−6
1.0	9	−9

The work reported here was conducted while both authors were faculty members at the Institute of Fluid Science, Tohoku University, Sendai, Japan. The authors would also like to thank the reviewers for their careful reading and helpful comments.

References

Bearman, P.W., Wadcock, A.J., 1973. The interaction between a pair of circular cylinders normal to a stream. Journal of Fluid Mechanics 61, 499–511.

Gaster, M., 1969. Vortex shedding from slender cones at low Reynolds numbers. Journal of Fluid Mechanics 38, 565–576.

Gaster, M., 1971. Vortex shedding from circular cylinders at low Reynolds numbers. Journal of Fluid Mechanics 46, 749–756.

Gerich, D., Eckelmann, H., 1982. Influence of end plates and free ends on the shedding frequency of circular cylinders. Journal of Fluid Mechanics 122, 109–121.

Hayashi, M., Sakurai, A., Ohya, Y., 1986. Wake interference of a row of normal flat plates arranged side by side in a uniform flow. Journal of Fluid Mechanics 164, 1–25.

Higuchi, H., Lewalle, J., Crane, P., 1994. On the structure of a two-dimensional wake behind a pair of flat plates. Physics of Fluids 6, 297–305.

Kim, H.J., Durbin, P.A., 1988. Investigation of the flow between a pair of circular cylinders in the flopping regime. Journal of Fluid Mechanics 196, 431–448.

Miau, J.J., Wang, G.Y., Chou, J.H., 1992. Intermittent switching of gap flow downstream of two flat plates arranged side by side. Journal of Fluids and Structures 6, 563–582.

Peschard, I., Le Gal, P., 1996. Coupled wakes of cylinders. Physical Review Letters 77, 3122–3125.

Piccirillo, P., Van Atta, C.W., 1993. An experimental study of vortex shedding behind linearly tapered cylinders at low Reynolds number. Journal of Fluid Mechanics 246, 163–195.

Spivack, H.M., 1946. Vortex frequency and flow pattern in the wake of two parallel cylinders at varied spacing normal to an air stream. Journal of Aeronautical Sciences 13, 289–301.

Sumner, D., Wong, S.S.T., Price, S.J., Païdoussis, M.P., 1999. Fluid behaviour of side-by-side circular cylinders in steady cross-flow. Journal of Fluids and Structures 13, 309–338.

Sumner, D., Price, S.J., Païdoussis, M.P., 2000. Flow-pattern identification for two staggered circular cylinders in cross-flow. Journal of Fluid Mechanics 411, 263–303.

Williamson, C.H.K., 1985. Evolution of a single wake behind a pair of bluff bodies. Journal of Fluid Mechanics 159, 1–18.

Zdravkovich, M.M., 1985. Flow induced oscillation of two interfering circular cylinders. Journal of Sound and Vibration 101, 511–521.